Quality Inspection System for Robotic Laser Welding of Double-Curved Geometries

Mikkelstrup, Anders Faarbæk; Thomsen, Mathias ; Stampe, Kristoffer; Endelt, Benny Ørtoft; Boll, Jens; Kristiansen, Ewa; Kristiansen, Morten

Published in:
Procedia Manufacturing

DOI (link to publication from Publisher):
10.1016/j.promfg.2019.08.008

Publication date:
2019

Document Version
Publisher's PDF, also known as Version of record

Available online at www.sciencedirect.com

ScienceDirect

Procedia Manufacturing 36 (2019) 50–57

Procedia MANUFACTURING

www.elsevier.com/locate/procedia

17th Nordic Laser Material Processing Conference (NOLAMP17), 27 – 29 August 2019

Quality Inspection System for Robotic Laser Welding of Double-Curved Geometries

Anders Mikkelstrup[a,*], Mathias Thomsen[a], Kristoffer Stampe[a], Benny Endelt[a], Jens Boll[b], Ewa Kristiansen[a], Morten Kristiansen[a]

[a] *Aalborg University, Department of Materials and Production, 9220 Aalborg, Denmark*
[b] *Grundfos A/S, 8850 Bjerringbro, Denmark*

Abstract

The quality of robotic laser welded parts is related to the joint location, the trajectory of the laser focal point and the process parameters. By performing in-process monitoring, it is possible to acquire sufficient process knowledge for post-inspection to evaluate the geometrical weld quality. The existing solutions for such systems operate along linear welds. This paper contributes with a quality inspection system for robot laser welding, that can handle double-curved geometries. The data acquisition system includes a CMOS camera, which is mounted such that it looks through the laser optics, external LED illumination and matching optical filters. During the process, the area around the moving laser focal point is captured, resulting in a sequence of images. The trajectory of the focal point is determined by estimating the 2D displacement field between each image using template matching and subsequently filtering the data through a Kalman filter to improve the accuracy and robustness of the system. The joint location is determined by applying a Canny edge detector and a standard Hough transform within a specified region of interest. As this paper deals with double-curved geometries, the region of interest is moved in relation to the laser trajectory, such that it always contains the visible part of the joint, that is closest to the focal point. The developed post-inspection system evaluates the quality of the weld by comparing the estimated trajectory relative to the determined location of the joint. The performance of the proposed quality inspection system was validated empirically on 18 samples. The tests showed promising results, as the system was able to accurately detect changes in the welding trajectory relative to the location of the joint with an accuracy of ± 0.2 mm.

Peer-review under responsibility of the scientific committee of the 17th Nordic Laser Material Processing Conference.

Keywords: Laser welding; Quality inspection; Image processing; Welding trajectory; Vision system

* Corresponding author. Tel.: +45 41 56 71 00.
E-mail address: afm@m-tech.aau.dk

2351-9789
Peer-review under responsibility of the scientific committee of the 17th Nordic Laser Material Processing Conference.
10.1016/j.promfg.2019.08.008

1. Introduction

High-power fiber laser welding is becoming increasingly popular in the mass-production industry for joining both ferrite and non-ferrite sheet metal plates due to its ability to produce a high-intensity heat source, that can be precisely focused onto a small area. This enables the possibility of producing keyhole welds at high speeds, while limiting the heat affected zone. A consequence of this is, however, strict tolerances to joint alignment and lateral positioning of the laser focal point to ensure structural integrity and fatigue life of the weld, especially in autogenous laser welding processes. In automated production set-ups, where the laser welding optics are manipulated by using a six-axis robot, the need for process monitoring and trajectory tracking is further emphasized. This is mainly due to positional inaccuracies in the robot's repeatability, especially along (complex) 3D welding trajectories at high speeds. [1, 2]

In the recent past, the topic of joint monitoring, seam tracking and online control of the laser welding process has been highly researched. Most published papers within this field of study have utilized a monitoring system containing similar key elements, which include an image sensor, a narrow band-pass filter, a powerful light source with a specific wavelength and in some cases a neutral density filter. [1, 3, 4].

M. de Graff, et al. [5] and W. Cieszyński, et al. [6] all used the aforementioned approach, coupled with common image processing techniques such as BLOB analysis and edge detection to analyze the laser welding process. With this type of monitoring system, they respectively succeeded in mapping and monitoring 3D butt joints, tracking the laser focal point and online correction of joint misalignment. R.-K. Zäh, et al. [7] and S. M. Portnov, et al. [8] proposed an alternative approach for monitoring of the laser welding process, utilizing a photo detector to detect emitted light from the process. These monitoring systems made it possible to set up a mathematical model of the laser welding process to improve control of deep penetration welds. In order to improve robustness of the laser welding vison-based monitoring systems, M. Nilsen, et al. [9] implemented a Kalman filter to estimate the joint gap, where the image processing had failed. This method turned out to improve robustness of the monitoring system and also reduced computation time, compared to other approaches. X. Gao, et al. [2] improved the robustness even further by combining a Kalman filter with a radial basis function neural network to account for dynamic colored noise, thereby improving the estimation capabilities of the Kalman filter.

2. Methodology

This paper deals with the challenge of acquiring a sufficient amount of robust process data for post inspection of laser welds, that have been performed along curved three-dimensional trajectories, as illustrated in Fig. 1. (a). More specifically, autogenous robotic laser welding of pre-worked thin stainless-steel metal plates. The aim is to detect changes in the welding trajectory in relation to the joint position, with the purpose of ensuring a stable and acceptable weld quality. The failure mode illustrated in Fig. 1. (b), is a result of short- and long-term process disturbances. Short term disturbances are defined as Gaussian noise, such as misplacement of the sub-components, while long term process disturbances are defined as time-dependent noise, e.g. temperature shifts or tool wear.

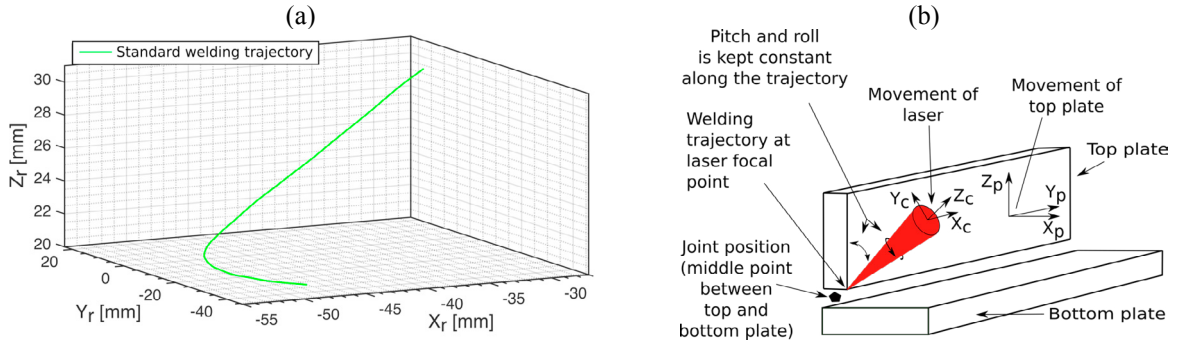

Fig. 1. (a) The green line indicates the curved three-dimensional welding trajectory of interest in the global coordinate system of the robot.; (b) The failure mode is defined as a misalignment in the welding trajectory in relation to the position the joint. The position of the joint is defined as the middle point between the top and the bottom plate.

The approach is based on an image sequence, captured with a CMOS camera through the laser optics during welding. The monitoring system proposed in this paper applies a combination of a Canny edge detector and a standard Hough transform to determine the joint position. Template matching is used to estimate the displacement field between subsequent image frames for computing the welding trajectory. To improve the prediction capability, precision and overall robustness of the estimations, a Kalman filter combined with a radial basis function, neural network, onwards referred to as a neural network, is incorporated into the monitoring system.

Validation of the monitoring system is done by comparing the welding trajectory and joint position from the monitoring system to a series of forward kinematic estimations of the welding trajectory. The quality inspection system should be able to detect shifts in the process, such as a varying joint position and an incorrect welding trajectory within a precision of ± 0.2 mm. This is based on the tolerances for joint alignment and lateral positioning of the laser focal point, required to obtain a sufficient weld quality for the material thickness. However, it should be noted, that a change in the position of the laser focal point in the axial direction (Z_c direction) of the laser is not considered to be within the scope of this paper.

3. Experimental set-up

The experimental set-up consists of a solid-state laser, a TruDisk 4001 by manufacturer Trumpf with a 200 µm LLK-D fiber delivery system. It is connected to a Permanova WT04 ST optics with a motorized twin spot unit, that is mounted on a KUKA KR 30 HA 6D robot. The robot is a high accuracy model from KUKA AG with a repeatability of ± 0.05 mm. The weld of interest in this paper is a double-curved T-joint configuration, illustrated in Fig. 2. (a), consisting of two 4301 austenitic stainless-steel plates with a thickness of respectively 2 mm and 1.5 mm for the bottom and top plate of the T-joint. To minimize heat induced distortions, the plates have been clamped during the welding operation. The weld is performed at a desired speed of 100 mm/s with no filler material and shielding gas, following the curved three-dimensional trajectory, illustrated in Fig. 1. (a).

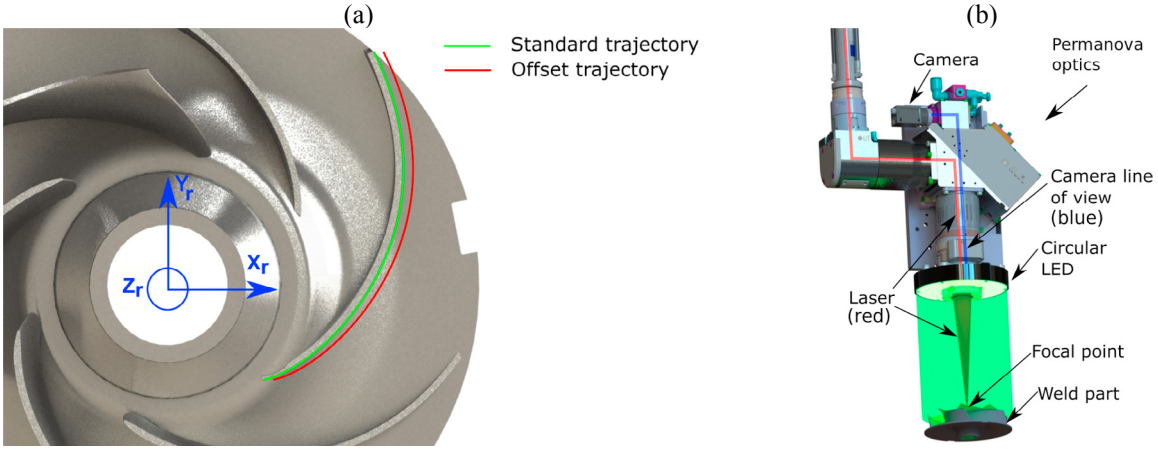

Fig. 2. (a) Presentation of offset in the standard welding trajectory; (b) Permanova WT04 ST optics with LED light source.

The experimental results were obtained by performing 24 consecutive welds to limit the amount of long-term process disturbances through two different tests scenarios. An overview of the different tests is presented in Table 1.

Table 1. Experimental test overview. All tests are conducted with the same laser spot size, collimation, test set-up and narrow-band-pass filter.

Test	Total welds	Welding speed	Average laser power	Offset	Collimation lens focal length	Focus lens focal length
1-3	18	100 mm/s	3100 W	No	180 mm	300 mm
4	6	100 mm/s	3100 W	Yes	180 mm	300 mm

The first three tests will be defined as standard weld and are performed to establish a reference for the performance of the monitoring system and to investigate the variance between identical samples. Subsequently, Test 4 is performed with a 1 mm offset in the X_r direction of the standard welding trajectory, as illustrated in Fig. 2. (a), in order to determine the detection capabilities of the monitoring system.

The optics presented in Fig. 2. (b) houses a built-in image acquisition system that includes a Basler acA645-100gm CMOS camera, mounted so its perspective is co-axial with the laser beam. This is illustrated in Fig. 2. (b). The camera has a frame rate of 100 fps and a resolution of 658 × 492 pixel in 8-bit grey scale. At the focus point, this results in a spatial resolution of 25 × 25 pixel/mm^2 minimize in-plane rotation and tilt of the camera, the pitch and roll are kept constant along the welding trajectory as illustrated in Fig. 1. (b). The image processing and the related operations are performed in MATLAB 2016b using an Intel Core i7-6700HQ CPU in combination with 16 GB of memory and a Radeon Pro 450 GPU.

An external light source has been mounted at the end of the Permanova optics, as illustrated in Fig. 2. (b). This is based on the monitoring system described in M. Nilsen, et al. [9]. By synchronising the trigger of the LED light to the exposure time of the camera, it has been possible to run a higher current through the LED light, thus increasing the light intensity in shorts bursts. In addition, matching optical filters consisting of a narrow band pass filter and a neutral-density filter have been mounted in front of the camera lens.

4. Signal processing

The signal processing deals with image processing of the camera signal to estimate the welding trajectory and joint position. In the following sections, *n* defines the total number of frames captured during the welding operation, while *k* defines the current frame, counted from the beginning of the captured welding operation.

4.1. Determining joint position using Canny detector and Hough lines

With the purpose of having some reference to indicate if the weld has been performed within the requirements, the $2 \times n$ joint position matrix $\mathbf{J}(k) = [x_c(k), y_c(k)]$ must be established. This is done through a six-step approach, illustrated in Fig. 3.

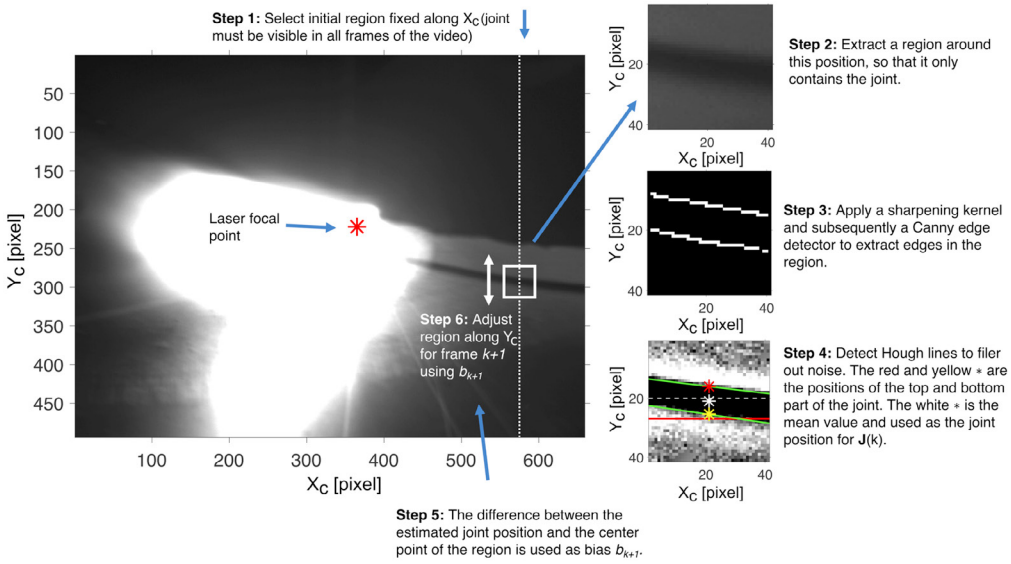

Fig. 3. Camera view with illustration of the steps for determining the joint position of the welding operation. The green Hough lines of step 4 indicate the lines with gradients within the limits, while the gradient of the red line exceeds the limits and is hence considered as noise. As an additional processing step, the joint position matrix **J**(k) is fitted with a 4th degree polynomial to minimize noise and predict missing data points. The above steps are iterated $k = k + 1$ to the next frame until $k = n$. [10, 11]

4.2. Estimation of welding trajectory using normalized cross-correlation template matching

Let Δx_c and Δy_c describe the camera's displacement field between subsequent video frames in respectively the X_c and Y_c direction in relation to the camera's moving coordinate system. The camera's displacement field is measured by selecting a region around the joint in frame k, similar to the procedure of step 2 in Fig. 3. The displacement of the region from frame k to $k + 1$ is then determined by performing normalized cross-correlation template matching between the two frames. The region around the joint is selected, as it is distinct and contains high intensity gradients, which are normally easier to track. As there is no in-plane rotation in the video frames, normalized cross-correlation template matching has proven to be more computationally efficient and robust to image noise, compared to more advanced feature matching methods, such as SURF, proposed by H. Bay, et al. [12].

The points defining the estimated welding trajectory $\mathbf{I}(k)$, can be estimated by summing up the displacement field for the previous frames of k, as stated by (1), where $\mathbf{U}(k) = [\Delta x_c(k), \Delta y_c(k)]$ is the displacement matrix.

$$\mathbf{I}(k) = \sum_{i=1}^{k} \mathbf{U}(i) \quad \forall k \leq n \tag{1}$$

4.3. Kalman filter for displacement field estimates

The displacement matrix $\mathbf{U}(k) = [\Delta x_c(k), \Delta y_c(k)]$ contains excessive noise primarily due to light disturbances from the laser beam. As a result, two separate discrete-time Kalman filters, one for X_c displacement Δx_c and one for Y_c displacement Δy_c is implemented. The two Kalman filters employ almost identical dynamic models to estimate the displacements, only differing in whether they make use of the values belonging to X_c or Y_c. (2) presents the state system equation for Δx_c. The state variables for the process model is chosen as the displacement field at sample k ($\Delta x_{c,1}$), the change in the displacement from $k - 1$ to k ($\Delta x_{c,2}$) and the displacement at $k - 1$ ($\Delta x_{c,3}$).

$$\mathbf{X}(k+1) = \begin{bmatrix} 1 & t & 0 \\ 0 & 1 & 0 \\ 1 & 0 & 0 \end{bmatrix} \begin{bmatrix} \Delta x_{c.1}(k) \\ \Delta x_{c,2}(k) \\ \Delta x_{c,3}(k) \end{bmatrix} + \begin{bmatrix} \frac{1}{2}\Delta t^2 \\ t \\ 0 \end{bmatrix} w_x(k) = \phi \mathbf{X}(k) + \Gamma w_x(k) \tag{2}$$

Where w_x(k) describes the system dynamic noise for Δx_c. ϕ and Γ being respectively the state transformations matrix and the noise drive matrix. The sampling rate Δt is determined by the frame rate of the camera, thus making $\Delta t = 0.01$ s for this application. The Kalman filters are implemented under the assumption that the weld is performed with a constant speed, and that the camera has a constant distance and angle to the surface of the component. The measurement equation then becomes:

$$\mathbf{Z}(k) = \begin{bmatrix} 1 & 0 & 0 \\ 1 & 0 & -1 \end{bmatrix} \begin{bmatrix} \Delta x_{c,1} \\ \Delta x_{c.2} \\ \Delta x_{c,3} \end{bmatrix} + \mathbf{V}(k) = \mathbf{H}\mathbf{X}(k) + \mathbf{V}(k) \tag{3}$$

In the traditional Kalman filter, the best estimation of the state vector $\mathbf{X}(k)$ relies on conditional variance information, which requires that the system dynamic noise $w_x(k)$ and sensor measurement noise $\mathbf{V}(k)$ are random uncorrelated Gaussian white noise models with zero mean and variances Q and **R**. However, according to X. Gao et al. [2], the $w(k)$ and $\mathbf{V}(k)$ of the welding process is colored instead of white. X. Gao, et al. [2] proposes to solve this challenge by driving Gaussian white noise through a shaping filter and introducing three associated coefficients λ, α and β. The coefficients λ, α and β and variances Q and **R** are used to tune the performance of the shaping filter and have been determined by a trial-and-error approach and are stated in Table 2.

Table 2. Coefficients λ, α and β and variances Q and **R** for the Kalman filters

	Q	**R**	λ	α	β
X_c	10	$[10^{-3}, 0; 0, 10^{-3}]$	0.3	0.1	0.1
Y_c	50	$[10^{-3}, 0; 0, 10^{-3}]$	0.3	0.1	0.1

In order to incorporate the colored noise into the Kalman filter, the approach of this paper applies the method proposed by X. Gao, et al. [2]. Hence incorporating the state system equation for Δx_c, stated by (2), the corresponding state system equation for Δy_c and the coefficients of Table 2. This will not be further outlined in this paper. The output of the Kalman filter is the corrected displacement matrix $\tilde{\mathbf{U}}(k) = [\Delta\tilde{x}_c(k), \Delta\tilde{y}_c(k)]$ that can be applied to determine the estimated welding trajectory, as by (1). $\Delta\tilde{x}_c$ and $\Delta\tilde{y}_c$ being respectively the corrected values of Δx_c and Δy_c.

4.4. Radial basis neural network displacement field prediction

The purpose of the neural network is to act as a more accurate predictor for the Kalman filter, where the image processing is not able to determine the displacement field. The evaluation criteria are defined as the gradient between the displacement field **U**(k) and the corrected displacement field $\tilde{\mathbf{U}}(k-1)$, which must not exceed a specified threshold ρ.

$$\left| \frac{\mathbf{U}(k) - \tilde{\mathbf{U}}(k-1)}{\Delta t} \right| < \rho \tag{4}$$

A standard three-layer radial basis function neural network is applied due to its generalization ability, stability and shorter training times, compared to many other neural networks. The input to the neural network is a $1 \times n$ vector **G**(k) containing the frame numbers $k = 1 \rightarrow n$ for the current video. The output is the predicted displacement matrix **U***(k), which is used instead of $\tilde{\mathbf{U}}(k)$ in cases, when ρ is exceeded. Training of the neural network follows the orthogonal least squares algorithm, which is employed as a forward regression method used to determine suitable radial basis function centers, as proposed by S. Chen, et al. [13]. The neural network is trained using $\tilde{\mathbf{U}}(k)$ as the target and **G**(k) as the input for the 12 most recent welds.

5. Validation and results

5.1. Geometrical coordinate transformations for system validation

Through a forward kinematic analysis, the KUKA software is able to estimate the position and hence trajectory of the laser focal point during the welding operation and will be used as a reference for comparison. As the image processing estimates the welding trajectory by calculating the trajectory based on the displacement field between subsequent frames from a moving camera, the trajectory is defined in relation to the coordinate system of each individual camera frame. The trajectory from the robot coordinate system is transformed to the moving image coordinate system by rotating the focal point coordinates from the trace analysis in the negative direction and in the opposite order of the angle-set convention, Z-Y-X Euler angles as $\mathbf{R}_{ZYX}$. Transforming the image coordinates (X_c, Y_c, Z_c) to the global coordinate system (X_r, Y_r, Z_r) of the robot is done using the same approach, however, in the original order of the angle-set as $\mathbf{R}_{XYZ}$.

5.2. Performance evaluation

By using the estimated welding trajectory, **I**(k) from the monitoring system, the position of the laser focal point can be compared to the joint position **J**(k) in the preceding frames. Fig. 4. (a) illustrates an image, where the visible area of the joint of each frame has been combined to form one single image by applying the corrected displacement matrix $\tilde{\mathbf{U}}(k)$. In addition, the estimated joint positions of **J**(k) have been plotted in the image for comparison. As

illustrated in Fig. 3., it is essential to note, that due to the large number of saturated pixels, it is not possible to directly compare the deviation between the laser focus point and joint in the same frame.

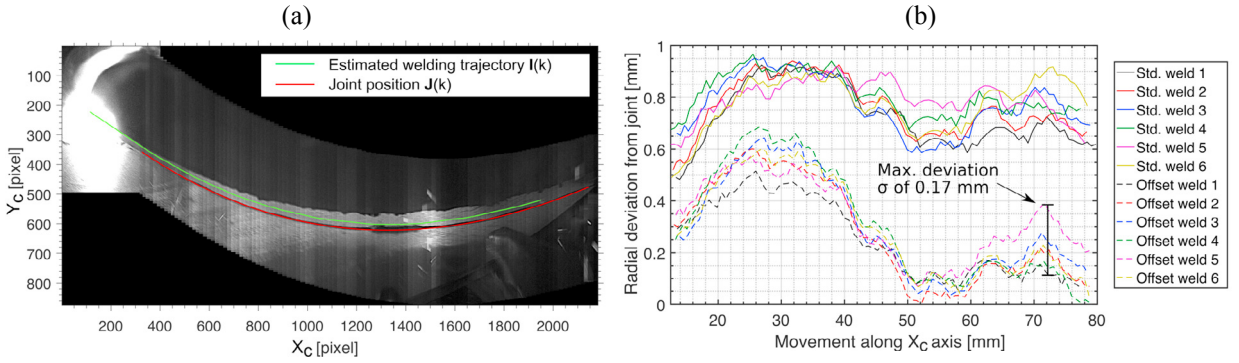

Fig. 4. (a) Visual comparison of the estimated welding trajectory and joint position in each frame of a standard weld. (b) Radial deviation of welding trajectories $\mathbf{I}(k)$ from the standard welds of Test 3 versus the offset welds of Test 4, compared to estimated joint positions $\mathbf{J}(k)$.

Fib. 4. (b) shows a comparison of six standard welding trajectories, in this case Test 3 of Table 1, and six offset trajectories from Test 4, all compared to their respective estimated joint position. The differences in the radial deviations of between the welding trajectories $\mathbf{I}(k)$, compared to estimated joint positions $\mathbf{J}(k)$, give an indication of the precision of the estimated welding trajectories and furthermore evaluates the system's ability to precisely detect process disturbances. The maximum deviation σ is 0.17 mm, which occurred on Test 3, as illustrated in Fig. 4. (b). By computing the deviation between the estimated joint positions $\mathbf{J}(k)$ of six welds, it is possible to evaluate the precision and robustness of the joint locater. Fig. 5. (a) shows the difference in the Y_c coordinate of the joint positions for all frames from the videos of Test 3. The X_c coordinate of the joint is fixed in all frames and is therefore not considered. The joint positions are compared to a reference, that has been determined by a neural network. In this case, it is roughly a weighted average of all the joint positions. The results show, that the maximum deviation σ is within the requirements of ± 0.2 mm.

The deviation between the trajectory and the joint position in the Y_c direction of both the standard and the 1 mm offset weld is transformed into the global robot coordinate system. The results are illustrated in Fig. 5. (b).

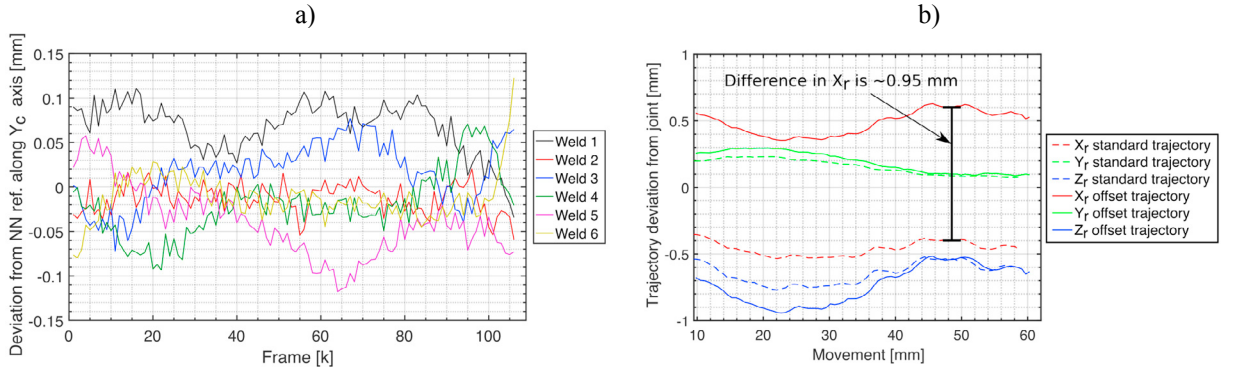

Fig. 5. (a) Deviation in the joint position $\mathbf{J}(k)$ of six welds compared to a neural network reference.; (b) Comparison of estimated standard trajectory $\mathbf{I}(k)$ versus estimated offset trajectory transformed into the global coordinate system of the robot.

The results indicate, that the mean offset ξ is approximately 0.95 mm in the X_r direction, which corresponds to the actual offset of 1 mm between the standard and offset weld. In addition, the results indicate a slight offset in both the Y_r and Z_r direction, which is likely a consequence of image noise and inaccurate synchronizing of the data from the forward kinematic analysis of the robot and the data from the quality inspection system.

The total cost time of the monitoring system, i.e. estimating joint position and welding trajectory for $n = 106$ frames, excluding loading of video and plotting is 3.05 s. For comparison, the welding operation elapses 1.16 s pr. weld.

6. Conclusion

This paper proposed a monitoring system to deal with the challenges of acquiring a sufficient amount of robust process data for post inspection of autogenous laser welds, that have been performed along curved three- dimensional trajectories. The monitoring system, purely rely on template matching for determining the frame displacement field showed promising results, however, it suffered from instabilities. To improve the system, it was extended to include a Kalman filter in combination with a radial basis function neural network to account for non-linear uncertainties in the Kalman filter. Based on the results presented in the previous section, when estimating the welding trajectory relative to the joint position, the monitoring system had a maximum deviation σ within the requirement of $\pm$ 0.2 mm between individual welds with a total cost time of 3.05 s. In addition, it was able to detect a mean offset ξ in the welding trajectory of 1 mm within an accuracy of $\pm$ 0.05 mm. The system should however be tested under a more extensive set of different scenarios to better evaluate the robustness and to further validate the monitoring system.

Replacing the implemented method for locating the joint with a convolution neural network could improve the accuracy, however at the expensive of an increased cost time in the form of network training. Implementation on a convolution neural network was investigated for this paper, but due to inadequate amount of training data, it was not possible to produce a detector, that outperformed the method. Another interesting aspect to investigate further is the possibility of measuring the displacement of the weld trajectory along the Z_c direction, the axial direction of the laser, by applying the principles behind stereo vision to estimate the depth parameter in the video.

Acknowledgement

A sincere thanks must be directed to Jens V. Boll, Peter T. Sørensen and Kenneth K. Meyer for their guidance and collaboration.

References

[1] W. Huang, R. Kovacevic, Development of a real-time laser-based machine vision system to monitor and control welding processes. International Journal of Advanced Manufacturing Technology, 63 (2012) 235–248.
[2] X. Gao, X. Zhong, D. You, S. Katayama, Kalman filtering compensated by radial basis function neural network for seam tracking of laser welding. IEEE Transactions on Control Systems Technology, 21 (2013) 1916–1923.
[3] W. Huang, R. Kovacevic, A laser-based vision system for weld quality inspection. Sensors, 11 (2011) 506–521.
[4] M. de Graaf, R. Aarts, B. Jonker, J. Meijer, Real-Time Trajectory Generation for Sensor-Guided Robotic Laser Welding, IFAC Proceedings Volumes, 39 (2006) 382-387.
[5] M. de Graaf, R. Aarts, B. Jonker, J. Meijer. Real-time seam tracking for robotic laser welding using trajectory-based control. Control Engineering Practice, 18 (2010) 944–953.
[6] W. Cieszyński, M. Zięba, J. Reiner, Real time trajectory correction system of optical head in laser welding. Acta Mechanica et Automatica, 9 (2015) 265–269.
[7] R.-K. Zäh, B. Mosbach, J. Hollwich, B. Faupel, Modelling and control for laser based welding processes: modern methods of process control to improve quality of laser-based joining methods. High-Power Laser Materials Processing: Applications, Diagnostics, and Systems VI, 10097 (2017) 100970A-100970A-13.
[8] S. M. Portnov, I. K. Israfilov, A. V. Perestoronin, A. G. Grigoryants, V. V. Zvezdin, A system for automatic control of precision laser welding in engineering. Welding International, 29 (2015) 801–804.
[9] Nilsen, M., F. Sikström, F., A. K. Christiansson, A. Ancona, Monitoring of Varying Joint Gap Width during Laser Beam Welding by a Dual Vision and Spectroscopic Sensing System. Physics Procedia, 89 (2017) 100–107.
[10] J. Canny, A Computational Approach to Edge Detection. IEEE Transactions on Pattern Analysis and Machine Intelligence, PAMI-8 (1986) 679-698.
[11] R.O. Duda, P.E. Hart, Use of the Hough Transform to Detect Lines and Curves in Pictures. Communication of the ACM ,15 (1972) 11-15.
[12] H. Bay, T. Tuytelaars, L. V. Gool, SURF: Speeded Up Robust Features, Computer Vision and Image Understanding, 110 (2006) 404-417.
[13] S. Chen, C.F.N. Cowan, P.M. Grant, Orthogonal least squares learning algorithm for RBF, IEEE Transactions on Neural Networks, 2 (1991) 302–309.